

Characterization of the Aging and Excess Noise of a Hamamatsu Fine Mesh Photopentode

D. Fujimoto*, C. Hearty

University of British Columbia, 6224 Agricultural Road, Vancouver, BC, V6T 1Z1, Canada

Abstract

The excess noise factor and the aging characteristics of 16 Hamamatsu R11283 photopentodes have been tested. These fine-mesh phototubes are to be paired with pure CsI scintillation crystals considered for use in the endcap calorimeter of the Belle II detector. The average excess noise factor was found to be $1.9 \pm 0.1 \pm 0.4$. The electronic noise of a custom preamplifier produced by the University of Montreal [1] was found as a consequence of this measurement and was 1730 ± 33 electrons, in agreement with previous values. On average, the gain \times quantum efficiency was reduced to 92 ± 3 % of the initial value after passing an average of 7 C through the anode. This corresponds to 70 years of standard Belle II operation.

Keywords: Hamamatsu, Photomultiplier, Mesh, CsI, Belle II, Aging

1. Introduction

One of the upgrade considerations for the Belle II detector, situated at KEK in Tsukuba, Japan, is to replace the current thallium-doped cesium iodide (CsI(Tl)) scintillation crystals in the endcap electromagnetic calorimeter (ECL) with pure CsI [2]. A primary goal of this exchange is to reduce pileup due to the increased luminosity of the SuperKEKB accelerator. While pure CsI has a shorter scintillation time constant, it also has a reduced light yield,

*Corresponding author.

Email addresses: fujimoto@phas.ubc.ca (D. Fujimoto), hearty@physics.ubc.ca (C. Hearty)

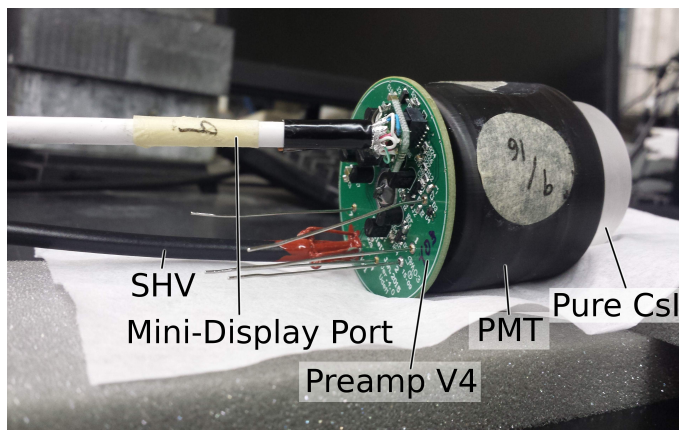


Figure 1: R11283 PMT with version 4 preamp produced by the University of Montreal [1] and glued pure CsI puck (AMCRYS) for the aging study. The preamp functions and output are powered and transmitted by a mini-display port cable, whereas the voltage divider has a SHV cable soldered to it.

with the emission spectrum peaking in the UV range rather than in the visible range [3, 4]. Therefore, the new crystals will need new photosensors. Under consideration for the new photosensor is the R11283 photomultiplier tube (PMT), developed by Hamamatsu Photonics for this project. This model has five flying leads and for this reason is often referred to as a photopentode. The PMT is a head-on type with three fine mesh dynodes, UV transparent window, and a bi-alkali photocathode; similar to previously tested PMTs for CsI scintillation crystals, although this model is of much lower gain and has fewer dynodes [5]. The photocathode of the R11283 has a minimum effective diameter of 39 mm, and a wavelength of maximum response of 420 nm [6]. Pure CsI has an emission maximum at 315 nm. The PMT is shown in Figure 1.

Magnetic fields decrease the performance due to changes in the inter-dynode electron path. These fine mesh PMTs will operate in the 1.5 T Belle II axial magnetic field, reducing the nominal gain by a factor of 3.5 [7]. The average nominal gain of the 16 PMTs at an operating voltage of -1000 V was 255 ± 11 . As summarized in Table 1, Hamamatsu provides a variety of measurements at -750 V with purchase.

Table 1: Average Hamamatsu quantities which were measured at -750 V and the PMT internal gain for a population of 16 PMTs.

Quantity	Average	Range
Anode Luminous Sensitivity ($\mu\text{A}/\text{lm}$)	14000 ± 1000	[8750.0, 26100.0]
Cathode Luminous Sensitivity ($\mu\text{A}/\text{lm}$)	83 ± 3	[69.3, 106.0]
Cathode Blue Sensitivity Index	9.4 ± 0.1	[8.70, 10.10]
Dark Current (nA)	0.011 ± 0.007	[0.00, 0.03]
Gain at -750 V	170 ± 7	[125, 276]
Gain at -1000 V	255 ± 11	[183, 367]

The PMT readout electronics were designed and produced by the University of Montreal [1] and consists of a preamp (version 4) and a shaper for every PMT. The preamp has a gain of 0.5 V/pC and the shaper has a shaping time of 50 ns. For a step-function input, the signal produced by the shaper has a peaking time of 200 ns. The combination of the two components produces a signal whose amplitude is proportional to the charge at the anode (Fig. 2). The board connected directly to the PMT (Fig. 1) houses both the voltage divider to power the PMT dynodes, and the preamp electronics. The shapers house and are powered by a motherboard which also provides the correct voltages to the preamp electronics.

Additional details on the measurements presented can be found in reference [8].

2. Methods

The shaper output was fed into a peak-sensing ADC (LeCroy L2259B) and the output was histogrammed using the MIDAS program [9]. The histogram was then fitted with the sum of an exponential and a Novosibirsk function. The exponential roughly describes the background, which was primarily due to backscatter. The Novosibirsk function is an asymmetric Gaussian-like function with four parameters: height, peak location, width, and an asymmetry parame-

ter [10]. Figure 3 shows an example of fitting this sum to the spectrum produced by the 662 KeV decay of ^{137}Cs .

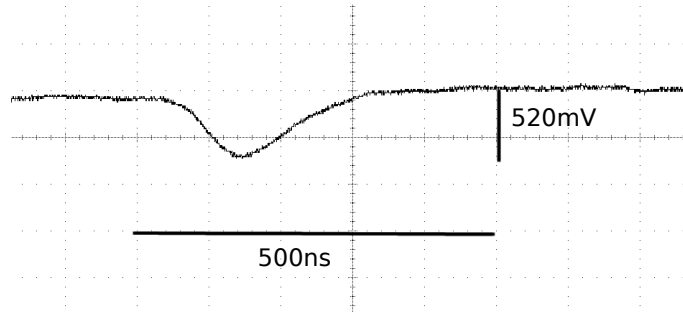


Figure 2: Typical single shot waveform produced by the University of Montreal shaper from a signal produced in pure CsI. The signal has a slightly longer peaking time due to the time constant of the scintillation material.

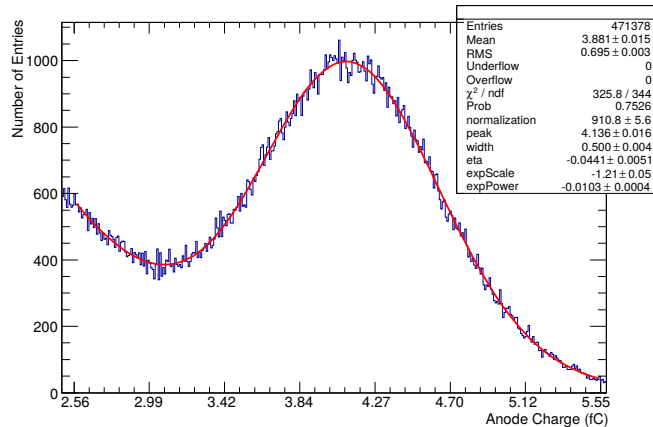


Figure 3: Histogram of peak-sensing ADC output with Novosibirsk + exponential fit for the spectrum produced by gammas from a ^{137}Cs source. A large background peak for anode charge less than 2.5 fC has been omitted for clarity.

The response of the system to energy deposits in pure CsI is linear. Using several calibration sources, the value of the peak location at zero energy deposited was extrapolated and attributed to a DC offset in the peak-sensing ADC. This pedestal was then subtracted from the measurements prior to any

further manipulation. The charge at the anode is proportional to the peak location, and the uncertainty to the width of this distribution. To calibrate the charge at the anode, the calibration test pulse feature of the preamp was used. This allows for a known amount of charge to be injected into the preamp, which is then processed as every other signal. From this calibration, the relationship between the ADC binning and the charge at the anode was found.

3. Excess Noise Factor

The excess noise factor is a common index for estimating the performance of photosensors [11]. This factor describes the uncertainty introduced into the system as a result of the electron multiplication process:

$$\left(\frac{\sigma_a}{N_a}\right)^2 = F \cdot \left(\frac{\sigma_c}{N_c}\right)^2, \quad (1)$$

where the subscripts c and a denote the cathode and anode respectively. Measured at location x , N_x and σ_x are the number of electrons and the signal width respectively, as determined from the Novosibirsk fit. F is the excess noise factor. Typically, the excess noise factor is larger for fine mesh PMTs than standard PMTs. Recognizing the Poisson nature of the photoelectrons and that the measured width at the anode contains contributions from both the constant electronic noise and the excess noise factor, Equation 1 can be written as:

$$\sigma_m^2 = F \cdot N_c + \sigma_o^2, \quad (2)$$

where the internal PMT gain has been applied to put all relevant quantities in units of number of electrons at the photocathode (photoelectrons). Here, σ_m is the measured width at the anode and σ_o is the contribution of the electronic noise. From this, the excess noise factor can be easily found by varying the light intensity (N_c) and measuring the resulting distribution width (σ_m).

To this end, a 405 nm UV laser was pulsed at 350 Hz to illuminate the PMT (Fig. 4). The laser was first reflected off of a diffusive white screen to provide uniform light. The light intensity was controlled via the laser voltage and the

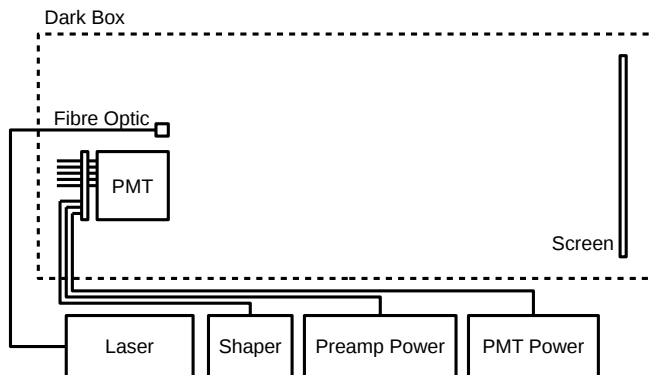


Figure 4: Setup for the excess noise measurement. A UV laser was reflected off of a screen to provide uniform incident light of controlled intensity.

screen-to-PMT distance. Using a single preamp, the excess noise factor was found for all 16 PMTs.

Figure 5 shows the results of this analysis for one of the PMTs. The slope is the excess noise factor, and the intercept is the electronic noise in units of photoelectrons. The operating voltage for these measurements was -1000 V. On average, the excess noise factor was found to be $1.9 \pm 0.1 \pm 0.4$, where the statistical error of 0.1 is the standard deviation across the 16 PMTs. The systematic error of 0.4 is due to the 25% uncertainty in the value of the capacitor used in the test pulse calibration [1]. The average electronic noise was 1730 ± 33 electrons at the anode, which is in good agreement with previous measurements [1]. The range of the excess noise factors was 1.8 – 2.1, whereas the range of the electronic noise was 1526 – 1913 electrons at the anode. Assuming that the light yield of the CsI crystal is 85 photoelectrons per MeV deposited [12], this electronic noise corresponds to an equivalent noise energy of about 80 keV.

To estimate the impact of magnetic fields on the excess noise, the PMT gain was reduced by lowering the operating voltage. Above a gain of 55, the PMT was seen to have a constant excess noise factor. Below this, the excess noise factor increases non-linearly with decreasing gain, rising to $3.5 \pm 0.1 \pm 0.4$ at a gain of 25. In comparison, two avalanche photodiodes (APD) from the

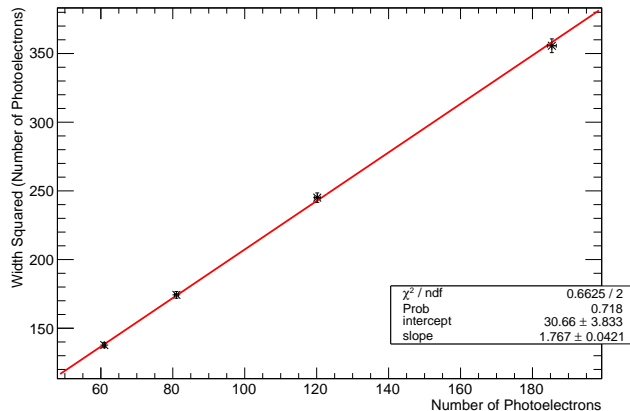


Figure 5: The excess noise factor is given by the slope of the fitted linear line as seen in Equation 2. The intercept gives the electronic noise in units of number of photoelectrons.

Hamamatsu S8664 series have been measured to have an excess noise factors of 3.4 and 5.1 [13]. These APDs are also being studied for pure CsI application as a competing option for the Belle II endcap ECL upgrade.

4. Aging

Of importance to the Belle II experiment is the effects of the PMT aging. Given that the Belle II endcap ECL will be in an axial magnetic field of approximately 1.5 T, and that the PMTs will be within 12.4° to 31.4° to this field [14], it is expected that the gain of the PMTs will drop by about a third [7]. To simulate this, the aging process was performed with the operating voltage of the PMTs set to -491 V, reducing the average gain to 85 ± 3 or one third of the nominal gain at -1000 V.

The performance of the PMT was characterized by the gain \times quantum efficiency, which was found from the slope of the peak ADC bin as a function of the energy deposited in the CsI. The change in the gain \times quantum efficiency relative to the initial value was monitored as a function of the charge passed through the anode, and also as a function of the real lab time elapsed. Light from a UV LED (335 nm) was used to age the PMTs, which were arrayed in a 4×4 array

(Fig. 6). The PMTs were encased in an incubator with a UV transparent acrylic window to maintain the temperature at 37 ± 2 °C. The relative humidity was kept within 15 – 20 % by means of desiccant and a slow influx of N₂ gas into the incubator. One of the 16 PMTs was capped with black rubber to prevent aging and act as a control. This PMT was also used to correct for the residual variation in temperature. The relative peak location response with temperature was roughly linear and varied at a rate of -1.2 ± 0.2 %/°C. Probably due to the poor thermal contact between dynodes and the environment exterior to the PMT, there is about a 8 – 10 hour delay before the PMTs reached thermal equilibrium.

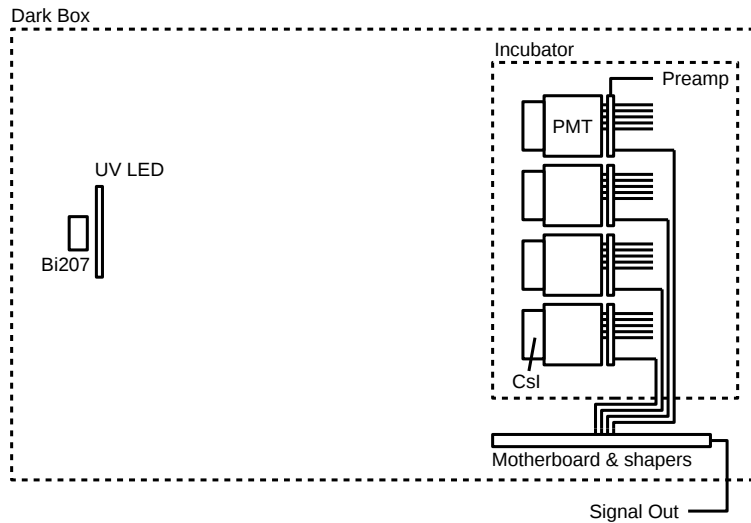


Figure 6: The experimental setup for the aging measurements. A 4×4 array of PMTs was encased in an incubator, with the temperature and humidity controlled. Aging was accelerated with a UV LED, and a ²⁰⁷Bi source was used to track the PMT performance.

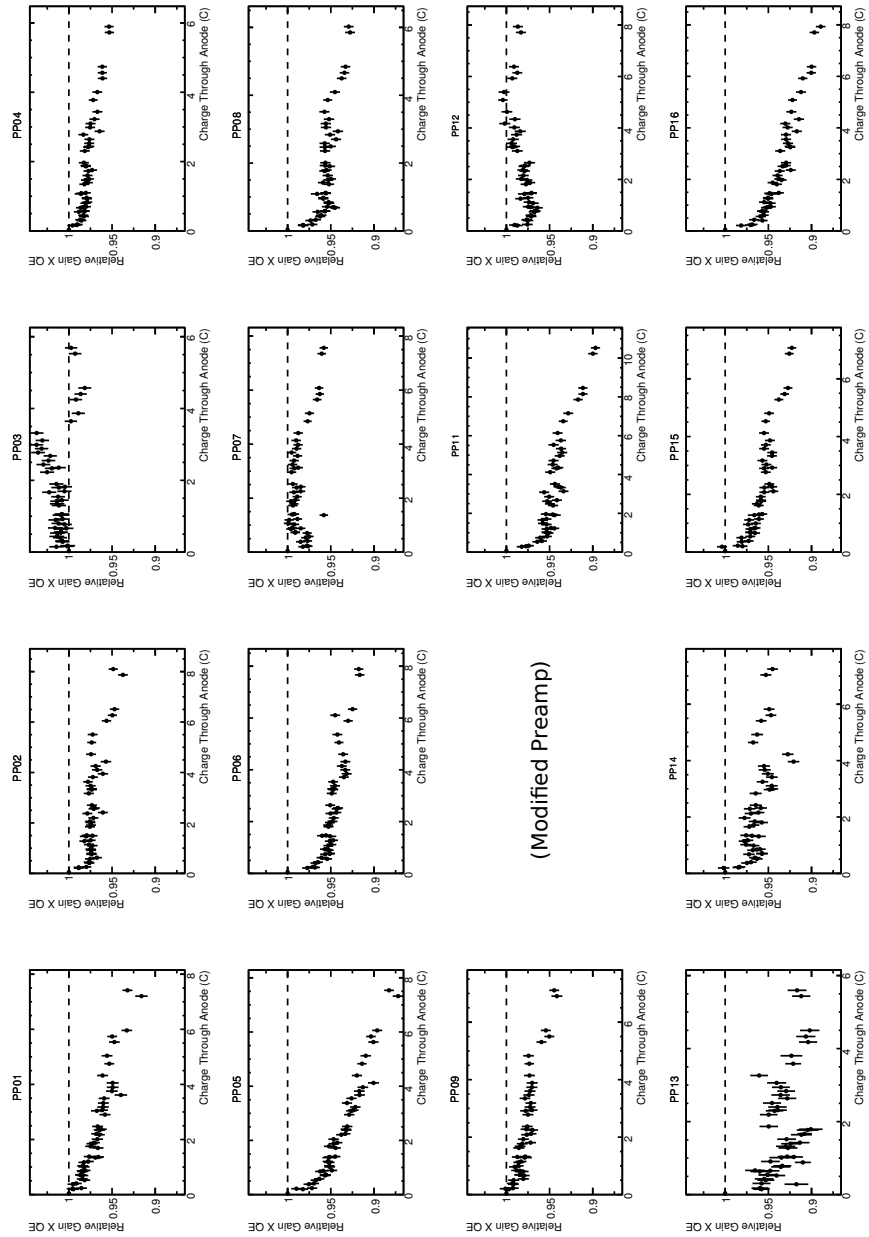
To track the performance, a constant light source was produced by gluing pure CsI pucks to the faces of the PMTs (Fig. 1) and triggering scintillation light with a ²⁰⁷Bi source. The glue used was TSE3032 silicone rubber produced by Momentive Performance Materials, which has an index of refraction of 1.406 for 589 nm light [15]. In comparison, the index of refraction of pure CsI is

1.95 at the emission maximum of 315 nm [3]. The CsI cylindrical pucks were manufactured by AMCRYST and were approximately the same diameter as the photocathode.

The measurement of the current was enabled by a modified preamp from the University of Montreal. This preamp did not perform any of the signal processing of the regular preamps, but rather contained a resistor such that the current could be measured with a Keithley 6485 Picoammeter. Prior to aging, a current baseline was established for each PMT using constant incident light. Using the baseline, only one PMT was needed to track the current through the anode and the current could be estimated for the other PMTs.

The ^{207}Bi source was chosen for its two easily visible decays at 0.570 MeV and 1.064 MeV. Given the linear response of the PMT with energy, these two peaks were used to establish the gain \times quantum efficiency, which can be seen as a function of the integrated current in Figure 7.

In Figure 7, the PMT in the third column of the first row (PP03) is the control PMT and was not aged. There are a few different observed behaviours in the PMT aging. Some exhibited a burn-in period where the performance decreased rapidly during the first coulomb of charge, then appeared to stabilize. Some appeared to age continuously throughout, whereas others exhibited little to no aging or even experienced an improvement in the performance. The control PMT did not see any significant change in performance at the end of the aging process.



(Modified Preamp)

Figure 7: PMT gain \times quantum efficiency relative to the first measurement, as a function of the charge passed through the anode, after temperature corrections. The horizontal dotted line marks the initial relative value of one. PP03 is the capped control PMT.

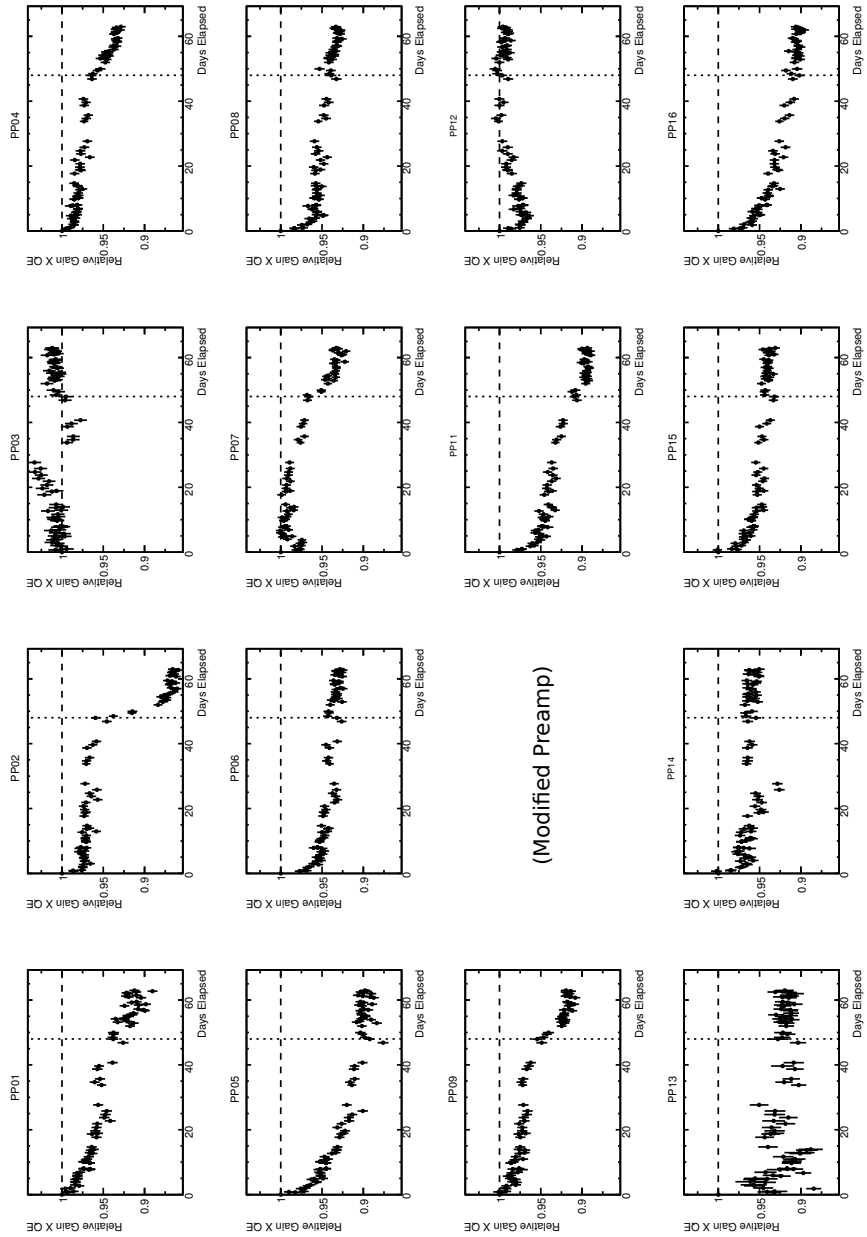


Figure 8: PMT gain \times quantum efficiency relative to the first measurement, as a function of lab time elapsed, after temperature corrections. The vertical dotted line marks the point where the UV LED was turned off and aging was halted. The horizontal dotted line marks the initial relative value of one.

After 48 days of aging, the LED was turned off and the stability monitored (Fig. 8). Even after aging, some of the PMTs continued to see a decrease in performance. Of note, one of the 14 aged PMTs (PP02) saw nearly 10 % decrease in performance within a week. This degradation is worrying as it is rapid enough to be difficult to track via a physics-based calibration system. The control PMT did not observe any significant change in performance after the end of the aging process. At the end of the aging process an average of 7.4 ± 1.2 C was passed through the PMT anodes and the average PMT performance was reduced to 92 ± 3 % of the initial value.

By definition, each PMT has a relative performance of 1 at zero charge. Other than at this point, the PMTs appear to be scattered normally about the mean (Fig. 9). Due to the internal gain of the PMTs, an equal amount of incident light does not produce the same number of electrons at the anode, and as a result there are fewer statistics available at the larger anode charges.

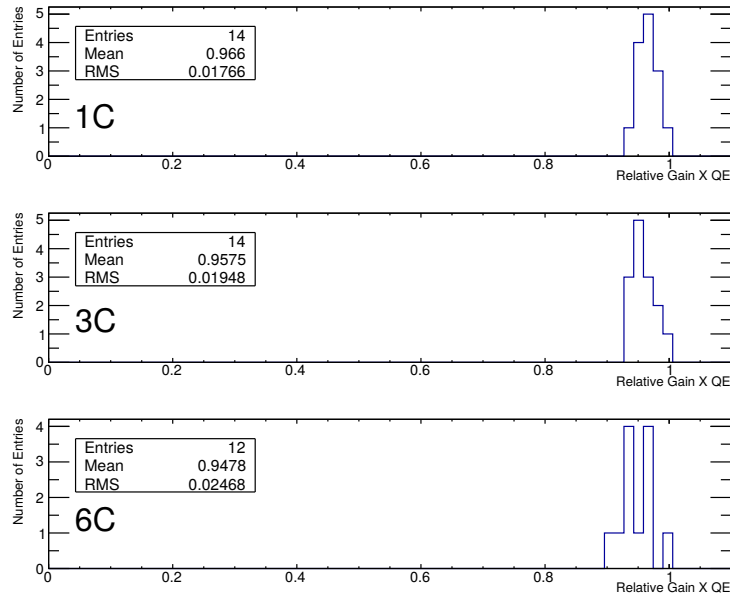


Figure 9: Histograms of the PMT gain \times quantum efficiency relative to the first measurement, at various stages in the aging process. The charge given is the anode charge after temperature corrections.

Figure 10 shows the average gain \times quantum efficiency as a function of charge, with an envelope denoting the RMS. These values were found by taking a linear interpolation to account for the gaps in the measurement. As mentioned earlier, not all of the PMTs saw an equal amount of charge. At 5.6 C, the total cumulative charge passed through the anode of the lowest gain PMT, the relative gain \times quantum efficiency was 95 ± 2 % across all 14 PMTs. As was seen in Figure 9, the RMS grows steadily with anode charge.

Empirically, the sum of a linear and exponential function was chosen to be fitted to the curve in Figure 10 in the range of $[0, 5.5]$ C, using the error in the mean as the fit weighting. The resulting function is given by

$$[\text{Rel. Gain} \times \text{QE}] = 0.968 - 0.0037q + 0.0383e^{-q/0.23}. \quad (3)$$

This shows that there exists a burn-in period, modelled by the exponential term, after which the PMT experiences a linear decay in performance of -0.4 %/C. The burn-in period lasts for 1.05 C, after which the exponential factor scales its coefficient by less than 1 %. By 1.57 C the exponential contributes less than 0.1 % to the function.

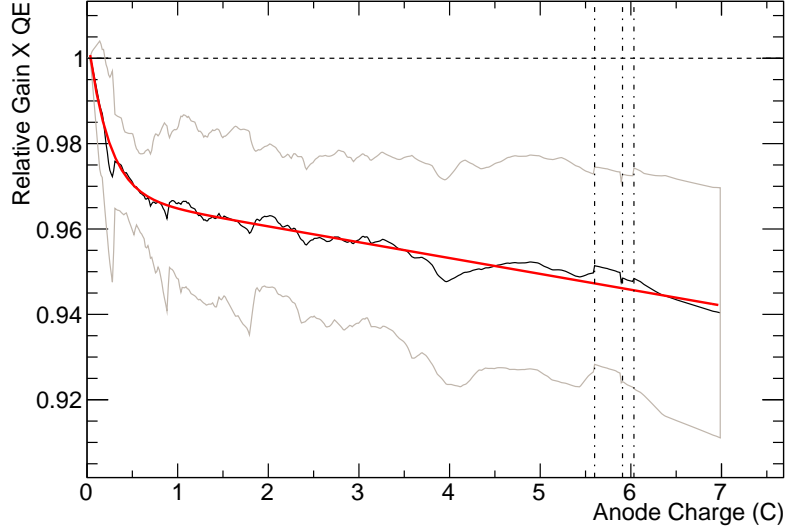


Figure 10: Average relative PMT gain \times quantum efficiency as a function of anode charge up to 7 C, with RMS envelope and functional overlay. The charge given is after temperature corrections, and the function is that of Eq. 3. The vertical lines denote where the number of PMTs present in the average drops by one (starting with 14). This occurs at 5.6 C, 5.9 C, and 6.0 C. Beyond 7 C the number of dropped PMTs increases rapidly.

5. Summary

The initial quantities measured by Hamamatsu prior to shipping can be found in Table 1. Using processing electronics developed by the University of Montreal, the excess noise factor and aging properties of the R11283 photopenode were studied. The average excess noise factor for 16 PMTs was found to be $1.9 \pm 0.1 \pm 0.4$ and the average electronic noise was measured to be 1730 ± 33 electrons at the anode. This electronic noise corresponds to an equivalent noise energy of 80 keV. The phototube aging was also studied by passing a large amount of charge through the anode, by exposing the photocathode to a large amount of incident light. At a reduced gain of 85 ± 3 , 14 PMTs were aged with an average of 7.4 ± 1.2 C passed through the anode, reducing the average performance of the PMTs to 92 ± 3 % of the initial measurement. Of the 14

aged PMTs, only one showed signs of rapid aging that could be a problem for some calibration systems. The average change in performance is characterized by an exponential burn-in period that lasts approximately 1.05 C, after which the performance degrades linearly by $-0.4 \%/C$.

Acknowledgements

This work was supported by the technical support staff at TRIUMF, in particular P. Amaudruz who developed the pulsed UV laser and aided in the setup of MIDAS. Additionally, J.P. Martin, N.A. Starinski, and P. Taras of the University of Montreal designed and produced the preamp, motherboard, and shaper electronics. D. Jow aided in the gluing of the CsI to the PMTs. Funding for this work was provided by NSERC.

References

References

- [1] J.P. Martin, N. Starinski, P. Taras, “Fast Charge-sensitive Preamplifier for Pure CsI Crystals”, Nucl. Instrum. and Methods A 778 (2015) 120.
- [2] Belle II collaboration, “Belle II Technical Design Report”, <http://xxx.lanl.gov/abs/1011.0352> (2011).
- [3] Saint-Gobain Ceramics & Plastics, Inc., “CsI(pure) Cesium Iodide Scintillation Material”, Tech. rep., accessed 03/08/15. <http://www.crystals.saint-gobain.com/uploadedFiles/SG-Crystals/Documents/CsI%20Pure%20Data%20Sheet.pdf> (2007).
- [4] Saint-Gobain Ceramics & Plastics, Inc., “CsI(Tl), CsI(Na) Cesium Iodide Scintillation Material”, accessed 03/08/15. [http://www.crystals.saint-gobain.com/uploadedFiles/SG-Crystals/Documents/CsI\(Tl\)%20and%20\(Na\)%20data%20sheet.pdf](http://www.crystals.saint-gobain.com/uploadedFiles/SG-Crystals/Documents/CsI(Tl)%20and%20(Na)%20data%20sheet.pdf) (2007).

- [5] T. K. Komatsubara, et al., “Performance of Fine-mesh Photomultiplier Tubes Designed for an Undoped-CsI Endcap Photon Detector”, Nucl. Instrum. and Methods A 404 (1998) 315.
- [6] Hamamatsu Photonics K.K. Electron Tube Division, “Photomultiplier Tube R11283 Technical Data”, Personal Communication (2013).
- [7] A. Kuzmin, “Endcap Calorimeter for SuperBelle based on Pure CsI Crystals”, Nucl. Instrum. and Methods A 623 (1) (2010) 252.
- [8] D. Fujimoto, “A Low Gain Fine Mesh Photomultiplier Tube for Pure CsI”, Master’s thesis, University of British Columbia (2015).
- [9] S. Ritt, et al., “Maximum Integrated Data Acquisition System”, <https://midas.triumf.ca> (1993).
- [10] H. Ikeda, et al., “A Detailed Test of the CsI(Tl) Calorimeter for BELLE with Photon Beams of Energy Between 20 MeV and 5.4 GeV”, Nucl. Instrum. and Methods A 441 (3) (2000) 401.
- [11] Hamamatsu Photonics K.K., “Photomultiplier Tubes: Basics and Applications” http://www.hamamatsu.com/resources/pdf/etd/PMT_handbook_v3aE.pdf (2007).
- [12] C. Hearty, “Pure CsI light output and resolution studies”, 17th Belle II General Meeting. <https://kds.kek.jp/indico/event/14531/session/73/contribution/251/material/slides/0.pdf> (2014).
- [13] Y. Jin, et al., “Study of a Pure CsI Crystal Readout by APD for Belle II End Cap ECL Upgrade”, Nucl. Instrum. and Methods A <http://dx.doi.org/10.1016/j.nima.2015.07.034>.
- [14] Belle collaboration, “The Belle Detector”, Nucl. Instrum. and Methods A 479 (2002) 117–232.

- [15] Momentive Performance Materials, “TSE3032 Technical Data Sheet”, accessed 08/07/15. <https://www.momentive.com/products/showtechnicaldatasheet.aspx?id=10404> (2015).
- [16] S. de Jong, “ECL backgrounds in the 11th campaign”, 20th Belle II General Meeting. <https://kds.kek.jp/indico/event/17439/session/30/contribution/256/material/slides/0.pdf> (2015)